AMERICAN SOCIETY FOR MICROBIOLOGY | Journal of Virology®

VACCINES AND ANTIVIRAL AGENTS

A Single Vaccine Protects against SARS-CoV-2 and Influenza Virus in Mice

Kangli Cao,[a,b] Xiang Wang,[b] Haoran Peng,[c] Longfei Ding,[b] Xiangwei Wang,[b] Yangyang Hu,[b] Lanlan Dong,[a] Tianhan Yang,[b] Xiujing Hong,[a] Man Xing,[d] Duoduo Li,[b] Cuisong Zhu,[b] Xiangchuan He,[a] Chen Zhao,[b] Ping Zhao,[c] Dongming Zhou,[b,d] Xiaoyan Zhang,[a,b] Jianqing Xu[a,b]

[a]Zhongshan Hospital & Institutes of Biomedical Sciences, Fudan University, Shanghai, People's Republic of China
[b]Shanghai Public Health Clinical Center, Fudan University, Shanghai, People's Republic of China
[c]Department of Microbiology, Second Military Medical University, Shanghai, People's Republic of China
[d]Department of Pathogen Biology, School of Basic Medical Sciences, Tianjin Medical University, Tianjin, People's Republic of China

Kangli Cao, Xiang Wang, Haoran Peng, and Longfei Ding contributed equally to this work. Author order was determined on the basis of strength of contribution.

ABSTRACT The ongoing SARS-CoV-2 pandemic poses a severe global threat to public health, as do influenza viruses and other coronaviruses. Here, we present chimpanzee adenovirus 68 (AdC68)-based vaccines designed to universally target coronaviruses and influenza. Our design is centered on an immunogen generated by fusing the SARS-CoV-2 receptor-binding domain (RBD) to the conserved stalk of H7N9 hemagglutinin (HA). Remarkably, the constructed vaccine effectively induced both SARS-CoV-2-targeting antibodies and anti-influenza antibodies in mice, consequently affording protection from lethal SARS-CoV-2 and H7N9 challenges as well as effective H3N2 control. We propose our AdC68-vectored coronavirus-influenza vaccine as a universal approach toward curbing respiratory virus-causing pandemics.

IMPORTANCE The COVID-19 pandemic exemplifies the severe public health threats of respiratory virus infection and influenza A viruses. The currently envisioned strategy for the prevention of respiratory virus-causing diseases requires the comprehensive administration of vaccines tailored for individual viruses. Here, we present an alternative strategy by designing chimpanzee adenovirus 68-based vaccines which target both the SARS-CoV-2 receptor-binding-domain and the conserved stalk of influenza hemagglutinin. When tested in mice, this strategy attained potent neutralizing antibodies against wild-type SARS-CoV-2 and its emerging variants, enabling an effective protection against lethal SARS-CoV-2 challenge. Notably, it also provided complete protection from lethal H7N9 challenge and efficient control of H3N2-induced morbidity. Our study opens a new avenue to universally curb respiratory virus infection by vaccination.

KEYWORDS COVID-19, vaccine, SARS-CoV-2 variants, influenza, adenoviral vector

In facing the COVID-19 pandemics caused by severe acute respiratory syndrome coronavirus 2 (SARS-CoV-2), the atlas of vaccination approaches has been exhaustively explored, resulting in nearly hundreds of vaccines in clinical stages, with several of them being applied to the human population in an effort to end the pandemics. However, the emergency of neutralizing antibody-escaping SARS-CoV-2 variants and the concern of SARS-CoV-2 becoming seasonal suggest the requirement of continuous effort for vaccine development. Given the pandemics of severe acute respiratory syndrome coronavirus (SARS-CoV) and Middle East respiratory syndrome coronavirus (MERS-CoV), along with the existence of other genera of coronaviruses (CoVs) known to infect humans (1), it would be beneficial to develop a vaccine that could universally

Editor Tom Gallagher, Loyola University Chicago

Address correspondence to Chen Zhao, chen_zhao72@163.com, Ping Zhao, pnzhao@163.com, Dongming Zhou, zhoudongming@tmu.edu.cn, Xiaoyan Zhang, zhangxiaoyan@fudan.edu.cn, or Jianqing Xu, xujianqing@fudan.edu.cn.

The authors declare a conflict of interest. J.Q.X., X.Y.Z., D.M.Z., K.L.C., X.W., Y.Y.H., and L.F.D. filed patents describing the invention and use of the vaccines described in the article. The other authors declare no competing interests.

Received 10 September 2021
Accepted 3 December 2021
Accepted manuscript posted online 15 December 2021
Published 23 February 2022

target CoVs. Before SARS-CoV-2, influenza A virus (IAVs) were the major viral cause of respiratory disease and posed a serious threat to global health and economy, as evidenced by the 1918 and 2009 H1N1 pandemic and, more recently, the 2013 H7N9 outbreak (2, 3). Influenza vaccines need to be administered annually, with efficacy varying from year to year and largely depending on the antigenic match between the circulating strains and the strains included in the vaccine (4), which are selected based on previous year's surveillance data (5). Another caveat of inactivated influenza vaccine is that its protection is majorly based on neutralizing antibody against viral hemagglutinin protein (HA) and the immunodominant head domain of HA is very tolerant to mutations introduced by antigenic drift mechanism (6), enabling antibody escape virus variants to arise (7). The antigenic shift caused by exchange of genetic materials between viruses coinfecting the same cell constitutes another mechanism for IAVs to thwart vaccine-mediated protection (8). Focusing the antibody response on the highly conserved stalk domain of HA has been thus proposed as a potential approach to develop a universal vaccine (9).

In the current study, we aim to develop a vaccine capable of providing dual protection against both SARS-CoV-2 and IAVs. We designed a synthetic immunogen by fusing the SARS-CoV-2 receptor-binding domain (RBD) to the conserved stalk of H7N9 hemagglutinin (HA) and expressed it using a chimpanzee adenovirus serotype 68 vector (AdC68). The constructed vaccine, named AdC68-CoV/Flu, was able to effectively induce both SARS-CoV-2-targeting antibodies and anti-influenza antibodies in mice, and consequently afforded protection from lethal SARS-CoV-2 and H7N9 challenges as well as effective H3N2 control. We propose AdC68-CoV/Flu as a novel two-in-one approach toward curbing respiratory virus diseases caused by SARS-CoV-2 and IAVs.

RESULTS

Immunogen design and vaccine construction. To develop a bivalent vaccine targeting both severe acute respiratory syndrome coronavirus 2 (SARS-CoV-2) and influenza A viruses (IAVs), we designed a fusion immunogen comprised of the receptor binding domain (RBD) of SARS-CoV-2 (amino acids [aa] 320 to 591) and the stalk domain (HA2) of hemagglutinin (HA) of the 2013 H7N9 virus (amino acids 340 to 524), which are linked by a multiple cloning site encoding 9 aa (VDELTSRGR). The immunogen construct began with an ER signal peptide, derived from murine IgGκ light chain at the N terminus of RBD, and ended with human ferritin at the C terminus of HA2 (Fig. 1A). In this tripartite design, ferritin is attached to the C terminus of immunogen to facilitate multimerization of HA2-RBD, owing to its natural capability of self-assembling into nanoparticles (NP) containing 24 monomers (10), thus allowing more effective engagement of antigen-specific B cells though multivalent interactions.

We chose AdC68 as the backbone to express our influenza-SARS-CoV-2 doubly-targeting immunogen because of its low preexisting immunity and overall safety profile (11, 12). Compared with human adenovirus serotype 5 (HuAd5), which has 75 to 80% seroprevalence, AdC68 has only 0 to 2% seropositivity in humans (13). The vaccine thus constructed was named AdC68-CoV/Flu. The recombinant AdC68-CoV/Flu vectored vaccine was produced in HEK 293A cells, purified by CsCl gradient ultracentrifugation, and subsequently quantified by absorbance measurement at 260 nm. To determine whether the immunogen could be effectively secreted, we infected the HEK 293T cells with 10^9 or 10^{10} viral particles (vps) of AdC68-CoV/Flu or AdC68 viruses in a 6-well format. After 24 h, cells and supernatants were analyzed for immunogen expression by Western blotting using a rabbit antibody specific for the S protein of SARS-CoV-2. As shown in Fig. 1B, we could detect the expression of the immunogen in the cell lysates but not in the supernatant. The observed molecular weight (approximately 90 to 95 kD) of the immunogen in Fig. 1B is larger than the theoretical size of the immunogen, which is 74 kD as computed from its protein sequence using the online ExPasy Molecular Server (http://us.expasy.org). To verify the glycosylation status of our immunogen, we performed a deglycosylation assay on purified ferritin-RBD proteins using

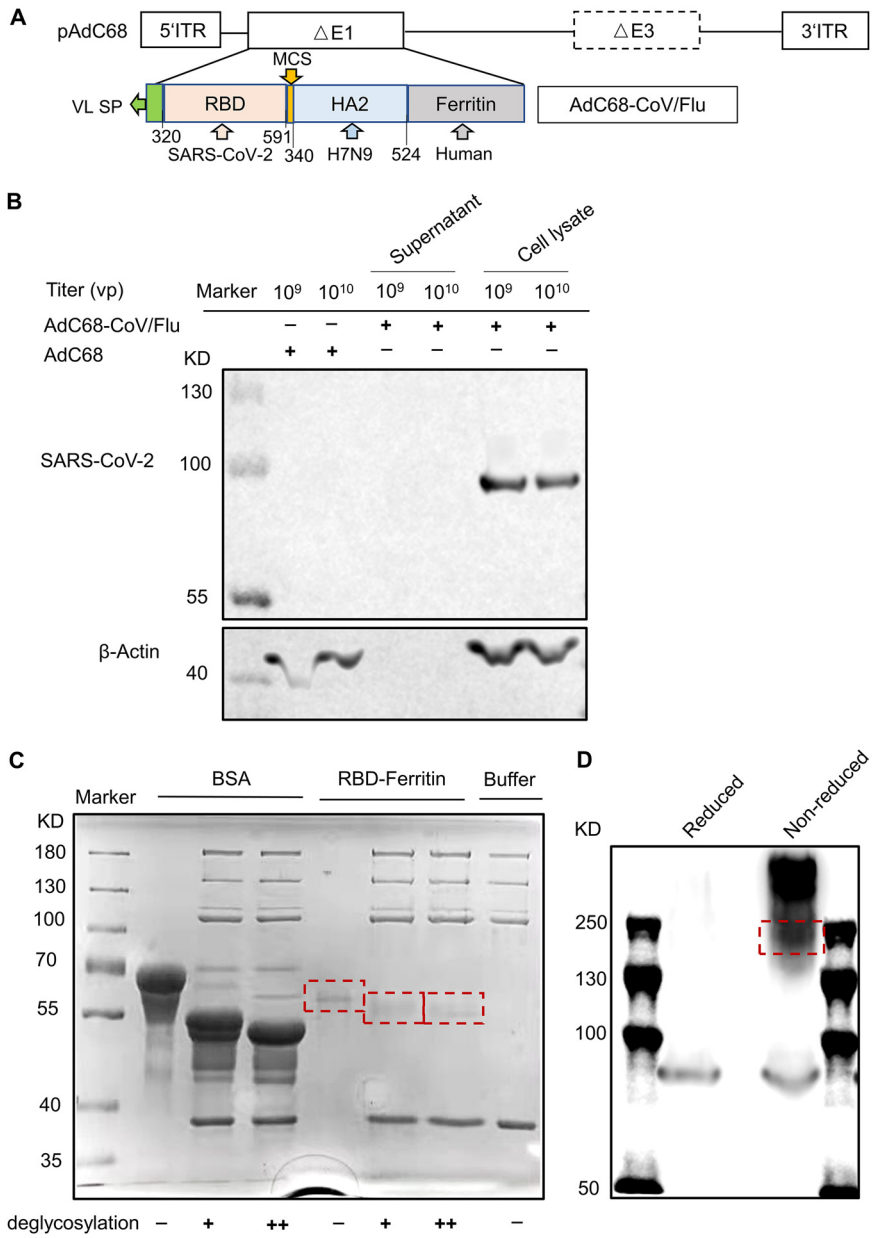

FIG 1 Construction of AdC68-CoV/Flu and verification of immunogen expression. (A) Schematic representation of design of AdC68-CoV/Flu, a vaccine intended to doubly target SARS-CoV-2 and influenza A virus. The fusion immunogen is comprised of three parts: RBD from SARS-CoV-2, HA stalk (HA2) from influenza H7N9, and human ferritin. (B) Verification of immunogen expression. HEK 293T cells were infected with the indicated amount (vps) of AdC68-CoV/Flu or AdC68 viruses in a 6-well plate and harvested 24 h postinfection. Resultant lysates were analyzed by Western blotting using a rabbit antibody specific for S protein of SARS-CoV-2. (C) Assessment of N-glycosylation of RBD. Purified BSA and RBD-ferritin proteins were treated or untreated with a deglycosylation mix under native conditions (+) versus more effectively denaturing conditions (++) and were then subjected to SDS gel electrophoresis. The separated proteins were visualized by Coomassie blue staining. (D) Verification of the structure of immunogen. HEK 293T cells were infected with 10^{10} vp of AdC68-CoV/Flu virus in a 6-well plate and harvested 24 h postinfection. Cell lysates were separated on SDS gel under reduced (+DTT) and nonreduced (-DTT) conditions and analyzed by immunoblotting using a rabbit antibody specific for S protein of SARS-CoV-2. The protein band with expected size of trimeric immunogen was marked by dashed rectangle.

BSA proteins as a positive control. The result, as displayed in Fig. 1C, showed they were indeed glycosylated. The shift in size caused by deglycosylation was consistent with the presence of two N-glycosylation sites (N331 and N343) in the RBD, as previously reported (14). Given that an individual N-glycosylation site is estimated to contribute

2.5 kDa in molecular weight, there should be other glycosylation sites in the immunogen from either HA2 or the ferritin portion. Indeed, HA2 was reported to contain one N-glycosylation site (15). We also analyzed the immunogen expressed in AdC68-CoV/Flu-infected 293T cells using Western blotting under nonreduced and reduced conditions to deduce the structure of the immunogen. The results indicated that although a small portion of the immunogens were in trimeric form (marked by a dashed rectangle), the majority of them were higher-order oligomers, consistent with the assembly of ferritin nanoparticle (Fig. 1D).

Humoral and cellular immune responses to AdC68-CoV/Flu vaccinated mice. We first evaluated the immunogenicity of AdC68-CoV/Flu in ICR mice following a two-dose homologous prime-boost vaccination regimen (Fig. 2A). A group of five mice received intramuscular injections of 5×10^{10} vp of AdC68-CoV/Flu vaccine at weeks 0 and 4. Also included was a control group receiving the same doses of empty AdC68 vector. Serum samples were collected at week 6 post-prime for analysis of antibody production using enzyme-linked immunosorbent assay (ELISA) and pseudovirus inhibition assay. As determined by ELISA, the RBD-binding antibody titers in the AdC68-CoV/Flu-vaccinated group ranged from 25,600 to 102,400 with a geometric mean titer (GMT) of 58,813 (left, Fig. 2B). Previous studies on the SARS vaccine indicated the importance of a balanced Th1/Th2 response for a successful vaccine, as a Th2 skewing was often linked to increased risk of vaccine-enhanced respiratory disease (VAERD). We thus also assessed the respective levels of IgG1 to IgG2a/c species—the ratio of the two values is widely accepted as a surrogate of Th1:Th2 polarization. The assessment revealed an average IgG2a/IgG1 ratio of approximately 1, with only one animal showing a value below 1, suggesting a beneficial antibody response that bore a low risk of VAERD (middle, Fig. 2C). The neutralizing antibody (nAb) titers by pseudovirus inhibition assay showed a range of 236 to 3,648 with a GMT of 692 (right, Fig. 2D). In contrast, neither RBD-binding nor neutralizing antibody titers could be detected in the control group.

Multiple SARS-CoV-2 variants with higher transmission potential have been identified in different geographic areas, including B.1.1.7 (United Kingdom), B.1.351 (South Africa), and B.1.1.28 (Brazil P1, P2) (16). B.1.351 is of particular concern because of its potential escape from antibody response induced by prior SARS-CoV-2 infection and vaccination (17). We hence assessed the serum nAb titers against different SARS-CoV-2 variants relative to the wild-type strain by pseudovirus inhibition assay at week 10 post-prime. The determined mean ratio of nAb titers of the B.1.1.7 variant to the wild-type strain was 1.09, indicating a non- or minimal loss in antibody neutralization. For B.1.351, we observed an average 40% reduction in nAb titers compared to the wild-type strain. However, this reduction was statistically insignificant, in line with the finding that the neutralizing activities induced by AdC68-CoV/Flu remained at least partially effective against this variant (Fig. 2E). Together, these results supported the potential of AdC68-CoV/Flu in engaging an effective antibody response against SARS-CoV-2 and its emerging variants.

Given the known strong potential of adenovirus in eliciting a T cell response specific to an inserted immunogen, we evaluated RBD-specific T cell responses of splenocytes isolated from immunized mice at week 5 ($n = 5$ per group) by an ELISpot assay that measured IFN-γ production after stimulation with pools of RBD-derived peptides. A total of 13 RBD peptide pools were used to fully cover the RBD sequence, each comprising five 15-amino acid peptides that overlapped by 11 amino acids. The aggregated T cell response to the entire RBD peptide pools, as reported in spot-forming cells (SFC) per 10^6 splenocytes, was robust in AdC68-CoV/Flu-vaccinated mice (GMT 4242, range 760 to 9,132) but was essentially undetectable in the control group (Fig. 2F). Measurements of T cell responses per peptide pool revealed reactivity in 10 out of the 13 pools (Fig. 2G); such an extensive T cell response may provide additional mechanism for blocking the escape of variants from neutralizing antibodies.

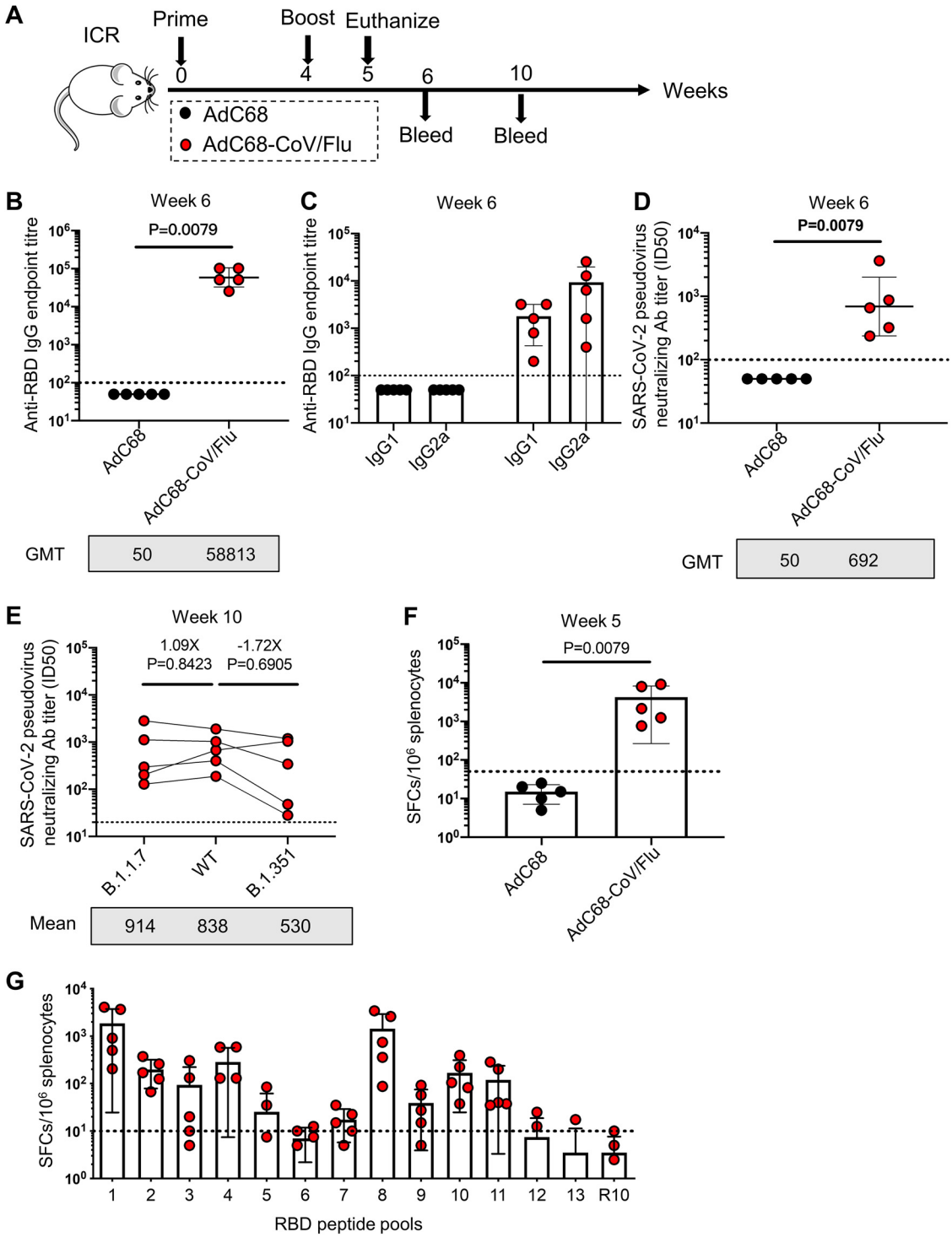

FIG 2 Immunogenicity of AdC68-CoV/Flu in mice. (A) Scheme of vaccination and sampling schedule. The mice were intramuscularly administered with AdC68-CoV/Flu or AdC68 in 5×10^{10} viral particles (vp) per dose following a homologous prime-boost regimen with a 4-week interval. (B) Serum were assessed by ELISA at week 6 post-prime for RBD-specific binding antibodies. (C) Assessment of Th1 or Th2 bias in the immune response. RBD-specific serum antibodies of IgG1 and IgG2a isotypes were determined by ELISA at week 6 post-prime, as their ratio serves as a surrogate measure of Th1/Th2 immune balance. (D) At week 6 post-prime, serum-neutralizing antibody titers against wild-type SARS-CoV-2 were measured by pseudovirus neutralization assays. (E) At week 10 post-prime, serum-neutralizing antibody titers against either wild-type SARS-CoV-2 or its B.1.1.7 and B.1.351 variants were assessed by pseudovirus neutralization assay. (F and G) Assessments of RBD-specific T cell responses. Splenocytes were isolated at week 5 post-prime and *in vitro* stimulated with 13 peptide pools (15-mer with 11 overlapped amino acids) covering the entire RBD sequence. The resulting IFN-γ secreting cells were quantified by ELISpot, recorded as a total response to the whole peptide pools (panel F) and individual peptide pools (panel G). Empty RMPI1640 complete medium, denoted as R10, was used as a negative

(Continued on next page)

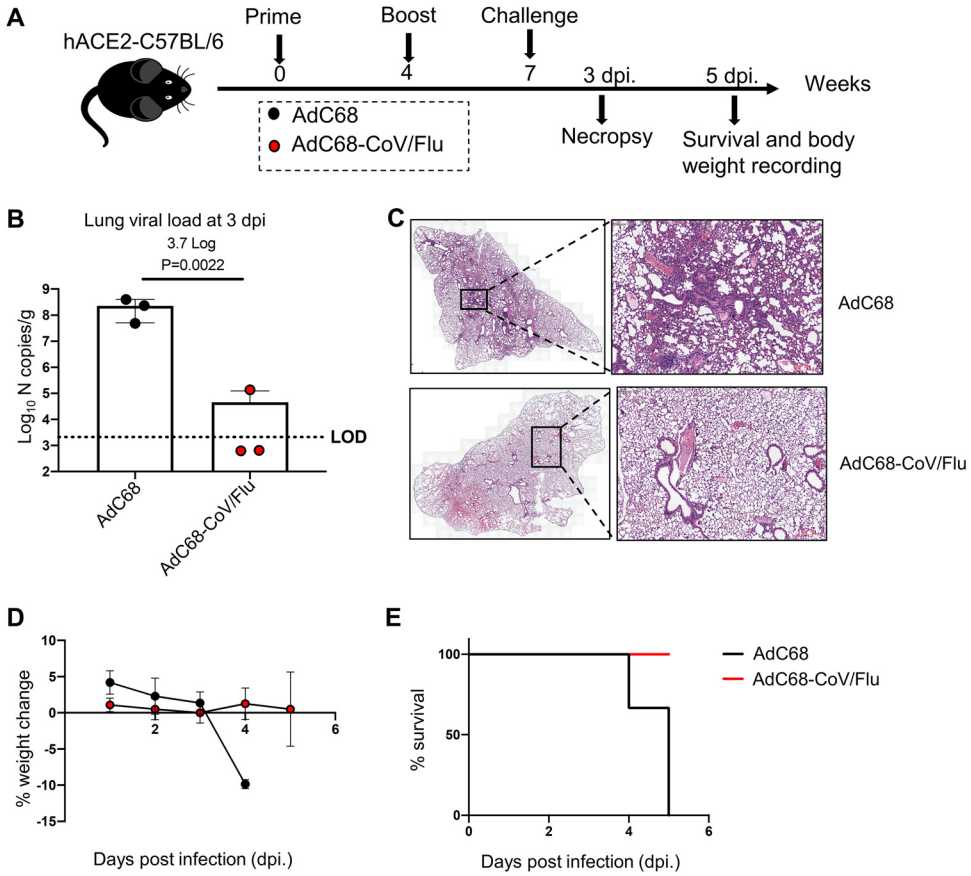

FIG 3 Protective efficacy of AdC68-CoV/Flu against SARS-CoV-2 challenge in hACE2 mice. (A) Experimental schedule. Transgenic hACE2-C57BL/6 mice (n = 8/group) were primed with intramuscular injections of 5×10^{10} vp of either AdC68 (sham) or AdC68-CoV/Flu on week 0, and 4 weeks later were boosted with 1×10^{11} vp of the same vaccine via both intramuscular and intranasal routes. This was followed by an intranasal challenge of 1×10^{4} PFU of SARS-CoV-2 (CHN/Shanghai_CH-02/2020) on week 7. (B) Lung viral loads on day 3 postinfection (dpi) were determined by quantitative RT-PCR of viral N transcripts in lung homogenates, which were plotted as $\log_{10}$ copies per mL. (C) Representative images of H&E-stained lung sections from AdC68- and AdC68-CoV/Flu-treated mice on 3 dpi. Scale bar, 200 μm. (D and E) Protection evaluated by % body weight change (panel D) and % survival (panel E). Between-group comparisons were conducted by Mann-Whitney tests.

Protection against lethal SARS-CoV-2 challenge by AdC68-CoV/Flu vaccine in hACE2-C57BL/6 mice. Next, we used hACE2 transgenic mice to examine the protective efficacy of AdC68-CoV/Flu vaccine against SARS-CoV-2 infection. hACE2-C57BL/6 mice (n = 10) were immunized with two doses of AdC68-CoV/Flu at week 0 (5×10^{10} vp by intramuscular route) and 4 (1×10^{11} vp by intramuscular and intranasal routes), followed by intranasal challenge with 10,000 PFU of SARS-CoV-2 (Fig. 3A). Lungs were harvested at 3 days postinoculation (dpi) for the assessment of viral loads and histopathology. Measurement of viral N transcripts by reverse transcription-quantitative PCR (RT-qPCR) showed a 3.7-log reduction of viral load in the AdC68-CoV/Flu-receiving animals compared to the control animals (Fig. 3B). H&E staining of lung tissue further revealed that AdC68-CoV/Flu vaccination ameliorated infection-induced pathology, minimizing bronchiolar epithelium disruption and markedly reducing the inflammatory infiltrates (Fig. 3C). Monitoring of body-weight changes and mortality consequently demonstrated the protection efficacy of AdC68-CoV/Flu. All the nontreated animals

FIG 2 Legend (Continued)
control. Titer data are presented as geometric mean titers (GMT) ± geometric standard deviation (GSD); ELISpot counts were expressed as mean ± standard error of the mean. A Mann-Whitney test was performed to analyze differences between experimental groups.

were dead after 5 days, accompanied by an abrupt reduction in body weight. Remarkedly, the vaccinated group did not show any signs of body weight loss, and all survived during the observation period (Fig. 3D and E). Thus, the AdC68-CoV/Flu was highly efficacious in protecting against SARS-CoV-2 infection in hACE2 mice.

HA targeting antibody response raised by AdC68-Cov/Flu and the resultant cross-subtype protection against H7N9 and H3N2 challenge in mice. After proving the CoV arm of AdC68-CoV/Flu, we sought to assess the other arm, which targets the HA stalk of influenza A virus. In this assessment, we used ICR mice and BALB/c mice, respectively, to examine the AdC68-CoV/Flu-mediated protection against the H7N9 virus, from which the HA stalk of AdC68-CoV/Flu was derived, and against the H3N2 virus, which also belongs to the group 2 viruses but features a HA that considerably differs from H7N9 HA. For the H7N9 testing, we adopted a two-dose prime-boost regimen, in which mice were immunized with two doses of AdC68-CoV/Flu or AdC68 at weeks 0 and 4 (5×10^{10} vp by the intramuscular injection route) before an intranasal challenge of 100,000 $TCID_{50}$ viruses of H7N9 at week 7 (Fig. 4A). The animals were first analyzed at 2 weeks post-boost for the serum antibody response. The AdC68-CoV/Flu-vaccinated sera showed high levels of H7-binding antibodies (GMT 19401, range 12,800 to 25,600), which were not detected in the samples from the sham controls (Fig. 4B). This robust antibody response translated to highly effective protection, as revealed by body weight and survival monitoring. In a sharp contrast to the AdC68-treated mice, which exhibited continuous weight loss starting from 1 dpi and consequently all succumbed to death before 10 dpi, the AdC68-CoV/Flu-vaccinated group was observed to have pronounced recovery from body weight loss displayed on earlier days post-challenge and it achieved 100% survival (Fig. 4C and D). For H3N2 testing, the same vaccination regimen was applied to BALB/c mice and the virus challenge was performed with intranasal inoculation of 500,000 $TCID_{50}$ viruses of H3N2 at week 8 (Fig. 4E). AdC68-CoV/Flu vaccination was able to induce a considerable level of H3-specific antibodies (GMT 350, range 200 to 800, Fig. 4F). This lower magnitude of induction compared with H7-specific antibodies was expected, as there is still significant sequence variation between the stalk regions from H3 and H7. Unlike the H7N9 virus, the H3N2 virus did not result in lethality in infected mice with the dose we used, and the AdC68-CoV/Flu protection was reflected by the fact that the AdC68-CoV/Flu vaccinated group consistently showed less weight loss than the sham-vaccinated group throughout the 14-day observation period (Fig. 4G). Thus, the Flu arm of AdC68-CoV/Flu was also functionally effective, with the capability to provide cross-protection against H7N9 and H3N2 viruses in mouse models.

DISCUSSION

In this study, we presented a strategy for the development of a single vaccine targeting two major respiratory viruses, SARS-CoV-2 and IAV. This strategy is implemented by the construction of a fusion immunogen comprised of the RBD domain of S protein from SARS-CoV-2 and the HA stalk region from influenza H7N9 virus, also using ferritin as a platform to improve the immunogenicity of the vaccine. The HA stalk is expected to serve multiple purposes: a conserved influenza domain for raising broad-spectrum anti-influenza antibody, acting as a scaffold to prevent RBD from collapsing onto ferritin, and potentially promoting the native RBD trimer formation (Fig. 1D) as a trimerization domain, facilitating the formation of antibodies against the conserved region. The use of a ferritin platform in vaccine development was first demonstrated with influenza HA and then extended to other viral antigens, such as the envelope glycoprotein (Env) of HIV (18). Studies on ferritin-based nanovaccines have demonstrated their superiority over conventional vaccines in gaining access to lymph nodes, packing efficiency, optimal antigen display, and elicitation of a sustained immune response. For example, Kanekiyo et al. originally showed that an HA-ferritin nanovaccine was able to induce high neutralizing titers in immunized animals that were approximately 34-fold higher than those of the commercially available, trivalent-inactivated influenza vaccine (TIV) (19). Both HA and Env are naturally trimers, making a case for the suitability of a

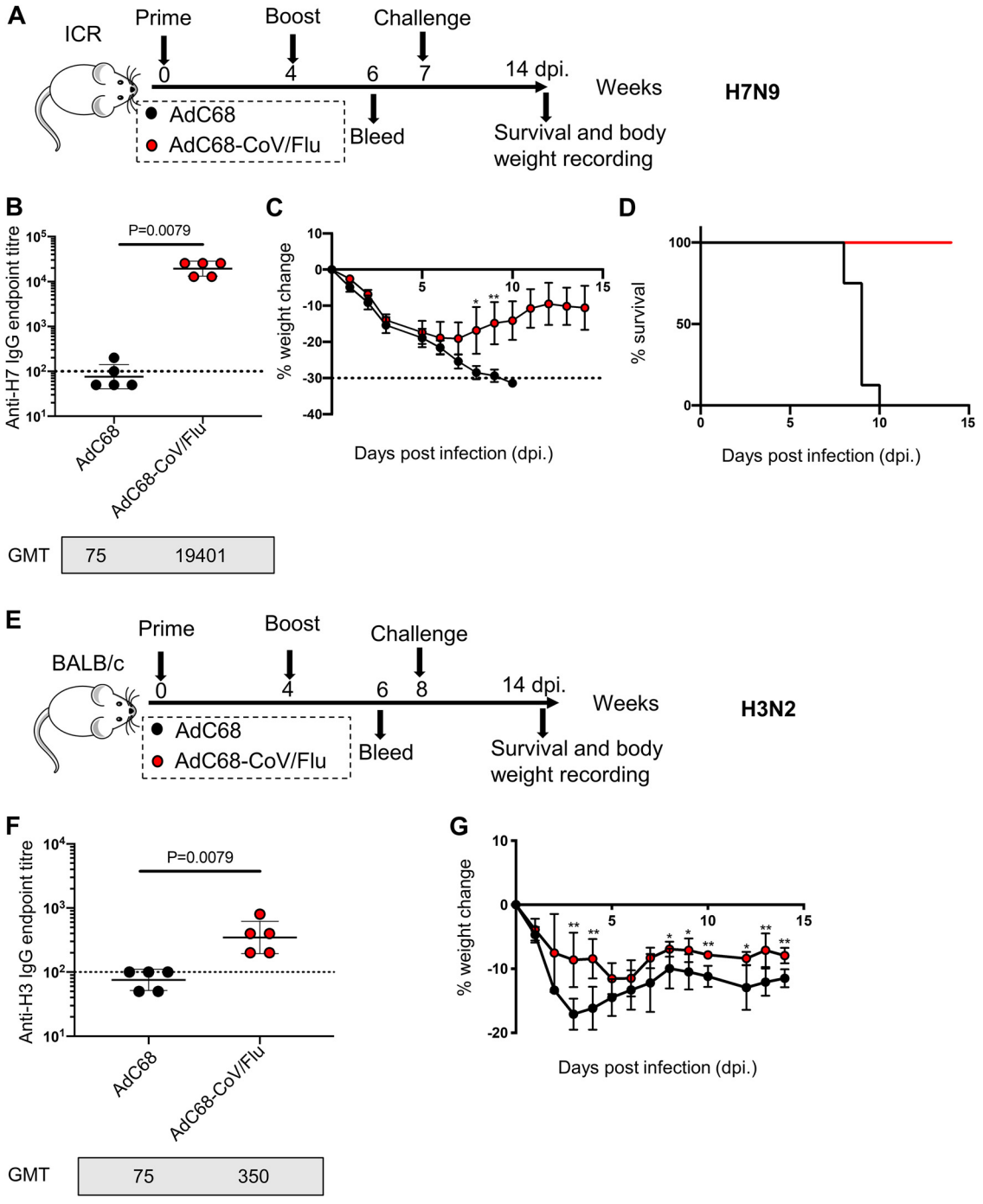

FIG 4 Influenza-targeting immunity raised by AdC68-CoV/Flu and the protection afforded against H7N9 and heterologous H3N2 challenges in mice. (A) Experimental schedule used for evaluating AdC68-CoV/Flu-mediated H7N9 protection. ICR mice (n = 5/group) were intramuscularly vaccinated with 5×10^{10} vp of either AdC68 (sham) or AdC68-CoV/Flu at weeks 0 (prime) and 4 (boost), followed by intranasal challenge with 1×10^{5} $TCID_{50}$ of A/Shanghai/4664T/2013 (H7N9) influenza virus at week 7. (B) Serum titers of H7 HA-specific binding antibodies at week 6 post-prime, determined by ELISA. (C and D) Protection evaluated by % body weight change (panel C) and % survival (panel D). (E) Experimental schedule used for evaluating protective efficacy of AdC68-CoV/Flu against H3N2 challenge. BALB/c mice (n = 5/group) were subjected to intramuscular vaccination with 5×10^{10} vp of either AdC68 or AdC68-CoV/Flu at weeks 0 (prime) and 4 (boost), followed by intranasal challenge with 5×10^{5} $TCID_{50}$ of A/Hong Kong/68 (H3N2) influenza virus H3N2 at week 8. (F) Serum titers of H3 HA-specific binding antibodies at week 6 post-prime, determined by ELISA. (G) Body weight change over time. Titer data are presented as geometric mean titers (GMT) ± geometric standard deviation (GSD). Between-group comparisons were conducted by Mann-Whitney tests.

ferritin platform for displaying RBD, a domain of the trimeric SARS-CoV-2 spike protein. It should be noted that there has been no preceding vaccine combining a ferritin platform with an adenoviral vaccine vector. Our characterization of our immunogen expressed in AdC68-CoV/Flu-infected cells showed that they mainly formed trimers and oligomers, supporting the facilitating role of ferritin in multimerization.

We showed that the AdC68-CoV/Flu vaccine was able to mount an antibody response against both SARS-CoV-2 and IAVs. Importantly, this response remained effective against B.1.351 with only a moderate decrease in neutralizing titers, which is in accordance with previous reports that RBD as an immunogen raised a broad neutralization antibody responses (20–23), whereas S protein mounted vigorous neutralization antibody responses against the wild-type strain but significant smaller responses against variants such as B.1.351, P.1, and B.1.627 (24–26), suggesting that RBD is likely to result in better exposure of conserved neutralization epitopes than S protein does.

In line with the antibody induction, AdC68-CoV/Flu vaccination effectively protected mice against both SARS-CoV-2 and influenza H7N9 challenges. AdC68-CoV/Flu vaccinated mice also showed decreased susceptibility to influenza H3N2 virus, substantiating our rationale of using the conservation of HA stalk to engage cross-reactive influenza-specific B cells. We noted that the H3N2 HA-binding titers was significantly lower than the H7N9 HA-binding titers, which was attributable to the sequence variation between stalks of the two HAs. This raises a concern about the efficacy of our vaccine in a human setting because H1N1 and H3N2 are the two major subtypes currently circulating in humans (27). However, pre-existing anti-influenza human immunity might provide a natural solution to this concern. Specifically, owing to the priming by seasonal virus/vaccine exposure, most humans are expected to possess a small repertoire of stalk-targeting cross-reactive memory B cells (28), which will be selectively activated and expanded once exposed to our vaccine and consequently potentiate protection efficacy. Indeed, our selection of H7N9 stalk was rationalized based on the remarkable breadth of HA-specific antibody responses exhibited by H7N9 patients (29), which led to the hypothesis that H7N9 stalk would be the optimal booster immunogen for inducing cross-group HA stalk antibodies.

Notably, AdC68-CoV/Flu vaccine can also induce potent RBD-specific T cell response in mice. This property might contribute to its protection against SARS-CoV-2 challenge according to the important role of T cell immunity in antiviral defense, which has been evidenced by the correlation between an early potent virus-specific $CD8^+$ T cell response and faster recovery of H7N9 patients (30) and longer persistence of virus-specific T cells than antibody response in recovered SARS-CoV-2-infected individuals (31–34).

One vaccination strategy as an alternative to AdC68-CoV/Fu is the combination of two AdC68-vectored vaccines individually expressing the SARS-CoV-2 RBD and H7 HA2 or the entire H7 HA ectodomain. We see that the AdC68-CoV/Flu vaccine offers several advantages over this rather traditional strategy. Firstly, as discussed above, fusion of RBD to HA2 might help stabilize both antigens in their native conformations, thus facilitating more effective induction of neutralizing antibodies. Secondly, compared to the entire ectodomain of H7 HA, H7 HA2 should be more compatible with RBD in inducing a balanced antibody response targeting the conserved epitopes of both immunogens. If H7 HA2 is replaced with the complete H7 ectodomain, the immunodominant H7 crown domain is expected to predominate in the immune response, resulting in less induction of H7 stalk-specific cross-reactive antibodies and possibly also attenuating the immunogenicity of RBD, which would consequently weaken the protective efficacy against SARS-CoV-2. Thirdly, in a human setting, the pre-existing T cell immunity against conserved epitope(s) of the H7 stalk region is likely to facilitate the initiation of an immune response against RBD. Lastly, but most importantly, a two-in-one vaccine solution is more cost-effective than a strategy requiring the production of two vaccines.

Several published pieces of evidence support the potential role of glycosylation of N343, and possibly also N331, in modulating the receptor-binding activity of RBD.

N343 glycosylation is speculated to conceal the receptor-binding sites, especially when the receptor binding domain adopts the "down" conformation (14). On the other hand, ablation of both N331- and N343 glycosylation drastically reduced the infectivity of SARS-CoV-2 (35), suggesting that the glycosylation on RBD is unlikely to shield the exposure of receptor binding domain in the "up" conformation. In addition, glycosylation of the RBD-neighbored domain may help to focus immune responses on RBD itself and thereby improve the neutralization antibody responses.

It should be noticed that the CoV/Flu immunogen presented in this study is a rationalized design based on known knowledge of its component parts and may be subjected to further optimization. For example, the current format of immunogen is nonsecreted; and, as known, secreted immunogen is able to induce stronger antibody responses than the nonsecreted one (36). We speculate that the poor secretion of immunogens might be attributed to their tendency to form high-order oligomers that are driven by ferritin; it is possible that the inclusion of ferritin, though facilitating the formulation of RBD trimers, may also result in compromised immunogenicity, and a secreted or membrane version is worth further exploration. Overall, AdC68-CoV/Flu opened new opportunity toward tackling respiratory diseases caused by SARS-CoV-2 and influenza A viruses, by setting the first example of two-in-one vaccine solution that is effective in animal models.

MATERIALS AND METHODS

Study design and animals. The primary objective of this study was to characterize in mice the immunogenicity and efficacy of a dual-targeting vaccine, AdC68-CoV/Flu, which was derived from chimpanzee adenovirus serotype 68 (AdC68) and expresses a fusion immunogen comprising receptor binding domain (RBD) of spike protein of SARS-CoV-2 and stalk domain of H7N9 hemagglutinin (HA). The AdC68-CoV/Flu vaccine was examined in mice using a homologous prime-boost regimen via intramuscular inoculation. Animals were randomly assigned to experimental and control groups, with the end points being pre-specified or based on the morbidity shown during the study and in some cases were selected according to the primary objective of immune response characterization. All animal experiments in this study were approved by the Institutional Animal Care and Use Committee (IACUC) of Shanghai Public Health Clinical Center and Second Military Medical University (SMMU). Pathogen-free 6-week-old female ICR and BALB/c mice, purchase from Shanghai Jihui biological Co., Ltd., were housed in the animal facility of Shanghai Public Health Clinical Center (SPHCC). 6-week-old female human angiotensin converting enzyme 2 (hACE2) transgenic C57/BL6 mice used for SARS-CoV-2 challenge were obtained from Shanghai Model Organisms Center, Inc., and maintained at BSL-3 laboratory in the Second Military Medical University (SMMU) during the study period.

Cell lines and viruses. The cell lines used in this study include human HEK 293A, human HEK 293T, monkey Vero E6, and canine MDCK. All of these cell lines were purchased from American Type Culture Collection (ATCC) and maintained in complete Dulbecco's modified Eagle's medium supplemented with 10% fetal bovine serum (FBS) and 1% penicillin-streptomycin (PS) at 37°C in a 5% CO_2 incubator. The generation of wild type SARS-CoV-2 pseudovirus was described in our previous publication (37, 38) and pseudoviruses carrying B.1.1.7 or B.1.351 variants were generated following the same procedures. The SARS-CoV-2 CHN/Shanghai_CH-02/2020 strain (GenBank: MT627325.1) was propagated and titrated using Vero E6 cells. The influenza A/Shanghai/4664T/2013 (H7N9) virus (GenBank accession numbers: KC853225.1, KC853226.1, KC853227.1, KC853228.1, KC853229.1, KC853230.1, KC853231.1, KC853232.1) and A/Hong Kong/68 (H3N2) virus (GenBank: EF409245.1) were propagated in 10-day-old embryonated chicken eggs and the tissue culture infectious dose ($TCID_{50}$) of virus stock was determined on MDCK cells.

Construction, rescue, propagation, and purification of recombinant chimpanzee adenoviruses. The vaccine, namely, AdC68-CoV/Flu, was generated in this study using recombinant chimpanzee adenoviral vector AdC68 as backbone. Different from wild-type AdC68, the recombinant AdC68 has both E1 and E3 genes deleted. For vaccine construction, the designed chimeric B cell immunogen sequence, featuring HA stalk derived from influenza A/Shanghai/4664T/2013 strain and RBD of wild-type SARS-CoV-2, was synthesized and cloned into E1 of recombinant AdC68 vector, with the help of a shuttle vector as described previously. The E1 locus is essential for viral replication and therefore recombinant AdC68 viruses can only be produced in cell line engineered to supply E1 protein, such as HEK 293A. The rescue, propagation, and purification of the three recombinant AdC68 viruses was performed as described previously. In brief, HEK 293A cells were seeded in 6-well plate and 24 h later transfected with PacI linearized corresponding AdC68 construct by Lipofectamine 2000 following manufacturer's instruction (Invitrogen, Carlsbad, CA). The rescued viruses were propagated in HEK 293A cells and purified using CsCl gradient ultracentrifugation in combination with desalting with Bio-Gel P-6 DG Media (Bio-Rad, USA).

Detection of immunogen expression by Western blotting. HEK 293T cells were seeded on 6-well plate and 24 h later infected with various amount of AdC68-CoV/Flu or AdC68 (10^9 and 10^{10} vps per well). After 24 h' further incubation, cells and supernatant were harvested and lysed in 100 μl RIPA buffer supplemented with a protease inhibitor cocktail. The resulting cell lysates and supernatant were

separated by SDS-page, followed by immunoblotting using a rabbit antibody specific for SARS-CoV-2 S protein (Sino Biological, 40591-T62). β-actin was also detected as loading control.

Protein deglycosylation. Protein deglycosylation were analyzed using a Protein Deglycosylation Mix II set (NEW ENGLAND Biolabs, #P6044) following the manufacture's protocol. In brief, under native conditions, the 100 μg of glycoproteins (BSA or RBD-Ferritin) were dissolved into 40 μl H_2O then add 5 μl 10$\times$Deglycosylation Mix Buffer 1. Next, add 5 μl Protein Deglycosylation Mix II, mix gently and incubate reaction at 25°C RT for 30 min. After that, transfer reaction to 37°C, incubate for 16 h. While under denaturing condition, 100 μg of glycoproteins (BSA or RBD-Ferritin) were dissolved into 40 μl H_2O then add 5 μl of Deglycosylation Mix Buffer 2, incubate at 75°C for 10 min, cool down. Next, add 5 μl Protein Deglycosylation Mix II, mix gently and incubate reaction at 25°C RT for 30 min. After that, transfer reaction to 37°C, incubate for 1 h. Finally, assess the extent of deglycosylation by mobility shifts on SDS-PAGE gels. The nondenatured reaction can then be compared to the denatured reaction to determine the extent of reaction completion.

Immunization and infection of mice. The mouse type, experimental schedule, and dosages of vaccines and challenging viruses were indicated in figures and their legends. Sera and spleen were collected from experimental animals for assessment of humor and cellular responses, respectively. For use in antibody determination, the sera were heat-inactivated at 56°C for 30 min. For T cell response assessment, the spleens were dissociated into single-cell suspension for peptide stimulation and following ELISpot analysis. During virus inoculations, animals were anesthetized with ketamine hydrochloride and xylazine to minimize suffering.

Enzyme linked immunosorbent assay. An enzyme linked immunosorbent assay (ELISA) was used to measure the RBD, H7, or H3 binding antibody titers of serum samples. In brief, 96-well ELISA plates were coated with 0.5 mg/mL of recombinant SARS-CoV-2 RBD protein (Genscript, Z03483-1), H7N9 H7 protein (Sino Biological, 40104-V08H) and H3N2 H3 protein (Sino Biological, 11972-V08B) at 4°C overnight. After washing the plates with PBS containing 0.5% Tween 20 (PBST) and blocking with 5% nonfat milk in PBST (PBST/5% milk) for 2 h at room temperature (RT), a 2-fold dilutions series (generally staring from 1:100) of mouse serum samples were added, followed by 3 h of incubation at RT. The plates were subsequently extensively washed with PBST before subjecting to total IgG measurement or separate assessments of IgG1 and IgG2. For total IgG measurement, a dilution of 1:5000 of HRP-conjugated goat anti-mouse IgG (Zsbio, ZB-5305) was applied in PBST/5% milk. After 1 h of incubation at RT, the plates were extensive washed with PBST before addition of the substrate OPD (one SIGMAFAST OPD tablet (Sigma, SLCC0308) in 20 mL of deionized water). The reactions lasted for 5 min at RT and were terminated by adding 1 M H_2SO_4, followed by reading at OD490 with a Synergy Microplate Reader (Bio-Tek, Winooski, VT). For the detection of IgG1 and IgG2, given lack of suitable HRP conjugated anti-mouse IgG1 and IgG2 antibodies, we first subjected the plates to 2 h RT incubation with rat anti-mouse IgG1, or IgG2 (1:2500 dilution; Biolegend, 406603 & 407103), which were then detected by 1 h RT incubation of HRP-conjugated anti-rat IgG (1:5000 dilution; Zsbio, ZB-2307) after extensive washing, with final step of color development performed as described above. ELISA endpoint titers were defined as the highest dilution that yields an absorbance of 2-fold greater than background value. Data analysis were conducted using GraphPad Prism 8.0.

IFN-γ ELISpot assay. T cell responses were analyzed using a mouse IFN-γ ELISpot assay set (BD Bioscience, #551083) following the manufacture's protocol. In brief, 96-well ELISpot plates were precoated with an anti-mouse IFN-γ antibody (5 μg/mL) overnight at 4°C. After rinsing with R10 culture medium-RPMI 1640 medium (Corning, 10 to 040-CVR) containing 10% fetal bovine serum (FBS) (BI, 04 to 001-1acs) and 1% penicillin-streptomycin (PS) (Corning, 30 to 002-CI), plates were blocked with R10 for 2 h at RT before adding to each well 2×10^5 of splenocytes, followed by stimulation with the indicated 15-mer peptide(s) or pool(s). Each assay was performed in duplicate. Peptide stimulation lasted 18 to 24 h as plates were placed in a humidified 5% CO_2 incubator at 37°C. The plates were subsequently washed twice with pre-cooled water and then 3 times with PBST before biotinylated anti-mouse IFN-γ antibody (2 μg/mL) was added for 2 h RT incubation. In the following step, streptavidin- conjugated horseradish peroxidase was added at 1:100 dilution and incubated at RT for 1 h. The plates were then washed with PBS and subjected to spot development with AEC substrate reagent (BD Bioscience, no. 551951), with the reaction being stopped by water rinsing and the plates subsequently allowed to dry 24 h in darkness. Plate images were captured with a Biospot plate reader (ChampSpot III, Beijing Sage Creation Science Co., Ltd.) and analyzed for spot-forming cell (SFC) counts.

Pseudovirus neutralization assay. The protocol for the generation of SARS-CoV-2 pseudovirus with a full-length SARS-CoV-2 spike protein (WT, B.1.1.7 or B.1.351) and a luciferase reporter gene was described in our previous publication (38). In brief, HEK 293T cells were cotransfected with pNL4-3.Luc.R-E- (NIH AIDS Reagent Program, cat no. 3418) and pcDNA3 plasmid encoding SARS-CoV2-S using TurboFect reagent (Thermo Scientific, cat no. R0531). Twelve hours posttransfection, the culture medium was refreshed with complete D10 medium for an additional 48 h of incubation. The pseudovirus-containing supernatants were then harvested, cleared by centrifugation, and stored at -80°C as single-use aliquots after filtering through 0.45 μm. For each pseudovirus stock, a titration assay was performed using an aliquot to determine the dilution needed for the neutralization assay. For assessment of serum-neutralizing activity against SARS-CoV-2, serial 50-μL dilutions of heat-inactivated serum were made with D10 medium and mixed with an equal volume of diluted pseudovirus. After incubation at 37°C for 1 h, the serum-pseudovirus mixtures were transferred to a 96-well plate containing hACE2-293T cells, which were preseeded at 2×10^4 cells per well and allowed to grow for 12 h. The plates were incubated for 48 h at 37°C in the presence of 5% CO_2 and luciferase activities were then measured using Bright-Glo Luciferase Assay System (Promega) on a luminometer (Promega GloMax 96). The neutralizing ID_{50} (50%

inhibitory doses) titers were derived from the highest dilution resulting in a 50% reduction in relative light units (RLUs) relative to virus-control wells after background (RLUs of no-virus wells) subtraction.

Quantification of viral loads by quantitative real-time PCR. Lung tissues of infected mice were pulverized and solubilized in TRIzol (Thermo). The contained RNA was purified using Direct-zol RNA Miniprep Plus kit (Zymo Research), and then subjected to random-hexamer-based cDNA synthesis using Maxima Reverse Transcriptase (Thermo). The resultant cDNA was subsequently assessed by SYBR Green-based RT-PCR analysis (GoTaq qPCR Master Mix; Promega, Charbonnieres, France) on a Bioer real-time PCR system using following N-specific primers: forward, 5′-GGGGAACTTCTCCTGCTAGAAT-3′; reverse, 5′-CAG ACATTTTGCTCTCAAGCTG-3′. The steps of PCR amplification included: 42°C for 5 min; 95°C for 10 s; 40 rounds of 95°C for 10 s and 60°C for 30 s. Quantification of the N transcript was based on a standard curve generated from measurements of serial dilutions of a reference plasmid encoding the full-length SARS-CoV-2 N gene.

Histopathology analysis. The lungs were fixed in 4% formalin and then embedded in paraffin, followed by cutting on a microtome to sections of 5-μm thickness. Sections were scanned using TissueFAXS Confocal Plus 200 (Tissue Gnostics) after staining with hematoxylin and eosin (H&E). The acquired images were analyzed by Strata Quest 6.0X software to assess lung pathology.

Statistical analysis. All statistical analyses were performed using GraphPad software (Prism V8.0, GraphPad). *P values* for difference between groups was determined by Mann-Whitney tests.

ACKNOWLEDGMENTS

We thank the members of the X.Y.Z. and J.Q.X. laboratories for advice and assistance during the study. We thank Zejun Li for the H7N9 virus and Bin Sun for the H3N2 virus.

The National Natural Science Foundation of China (81761128007, 81430030, 82071788), the National 13th Five-Year Grand Program on Key Infectious Disease Control (2017ZX10202102), the Shanghai Pujiang Program (19PJ1409100), and the Shanghai Science and Technology Commission (18DZ2293000) provided funding for this work.

J.Q.X. conceptualized and supervised the research. J.Q.X., X.Y.Z., D.M.Z., P.Z., C.Z., and K.L.C. designed the study and reviewed all data. K.L.C., X.W., H.R.P., L.F.D., X.W.W., Y.Y.H., L.L.D., T.H.Y., X.J.H., M.X., D.D.L., C.S.Z., and X.C.H. performed research. K.L.C. analyzed the data and wrote the original draft. J.Q.X., X.Y.Z., and C.Z. provided supervision and oversaw final manuscript preparation.

J.Q.X., X.Y.Z., D.M.Z., K.L.C., X.W., Y.Y.H., and L.F.D. filed patents describing the invention and use of the vaccines described in the article. The other authors declare no competing interests.

REFERENCES

1. Centers for Disease Control and Prevention (CDC). Human coronavirus types. https://www.cdc.gov/coronavirus/types.html.
2. World Health Organization (WHO). Influenza (Seasonal). https://www.who.int/en/news-room/fact-sheets/detail/influenza-(seasonal).
3. Lagacé-Wiens PRS, Rubinstein E, Gumel A. 2010. Influenza epidemiology-past, present, and future. Crit Care Med 38:e1-9. https://doi.org/10.1097/CCM.0b013e3181cbaf34.
4. Vestergaard LS, Nielsen J, Krause TG, Espenhain L, Tersago K, Sierra NB, Denissov G, Innos K, Virtanen MJ, Fouillet A, Lytras T, Paldy A, Bobvos J, Domegan L, O'Donnell J, Scortichini M, de Martino A, England K, Calleja N, van Asten L, Teirlinck AC, Tønnessen R, White RA, Silva SP, Rodrigues AP, Larrauri A, Leon I, Farah A, Junker C, Sinnathamby M, Pebody RG, Reynolds A, Bishop J, Gross D, Adlhoch C, Penttinen P, Mølbak K. 2017. Excess all-cause and influenza-attributable mortality in Europe, December 2016 to February 2017. Eurosurveillance 22:0–6. https://doi.org/10.2807/1560-7917.ES.2017.22.14.30506.
5. Gerdil C. 2003. The annual production cycle for influenza vaccine. Vaccine 21:1776–1779. https://doi.org/10.1016/s0264-410x(03)00071-9.
6. Tricco AC, Chit A, Soobiah C, Hallett D, Meier G, Chen MH, Tashkandi M, Bauch CT, Loeb M. 2013. Comparing influenza vaccine efficacy against mismatched and matched strains: a systematic review and meta-analysis. BMC Med 11. https://doi.org/10.1186/1741-7015-11-153.
7. Krammer F, Palese P. 2015. Advances in the development of influenza virus vaccines. Nat Rev Drug Discov 14:167–182. https://doi.org/10.1038/nrd4529.
8. Webster RG, Govorkova EA. 2014. Continuing challenges in influenza. Ann N Y Acad Sci 1323:115–139. https://doi.org/10.1111/nyas.12462.
9. Coughlan L, Palese P. 2018. Overcoming Barriers in the Path to a Universal Influenza Virus Vaccine. Cell Host Microbe 24:18–24. https://doi.org/10.1016/j.chom.2018.06.016.
10. Jiang B, Fang L, Wu K, Yan X, Fan K. 2020. Ferritins as natural and artificial nanozymes for theranostics. Theranostics 10:687–706. https://doi.org/10.7150/thno.39827.
11. Roy S, Gao G, Lu Y, Zhou X, Lock M, Calcedo R, Wilson JM. 2004. Characterization of a family of chimpanzee adenoviruses and development of molecular clones for gene transfer vectors. Hum Gene Ther 15:519–530. https://doi.org/10.1089/10430340460745838.
12. Vitelli A, Folgori A, Scarselli E, Colloca S, Capone S, Nicosia A. 2017. Chimpanzee adenoviral vectors as vaccines: challenges to move the technology into the fast lane. Expert Rev Vaccines 16:1241–1252. https://doi.org/10.1080/14760584.2017.1394842.
13. Farina SF, Gao G, Xiang ZQ, Rux JJ, Burnett RM, Alvira MR, Marsh J, Ertl HCJ, Wilson JM. 2001. Replication-defective vector based on a chimpanzee adenovirus. J Virol 75:11603–11613. https://doi.org/10.1128/JVI.75.23.11603-11613.2001.
14. Watanabe Y, Allen JD, Wrapp D, McLellan JS, Crispin M. 2020. Site-specific glycan analysis of the SARS-CoV-2 spike. Science 369:330–333. https://doi.org/10.1126/science.abb9983.
15. Liu W-C, Jan J-T, Huang Y-J, Chen T-H, Wu S-C. 2016. Unmasking stem-specific neutralizing epitopes by abolishing N-linked glycosylation sites of influenza virus hemagglutinin proteins for vaccine design. J Virol 90:8496–8508. https://doi.org/10.1128/JVI.00880-16.
16. Yadav APD, Sapkal GN, Abraham P, Ella R, Deshpande G, Patil DY, Nyayanit DA, Gupta N, Sahay RR, Shete AM, Panda S, Bhargava B, Mohan VK. 2021. Neutralization of variant under investigation B.1.617 with sera of BBV152 vaccinees 1–11. Clin Infect Dis https://doi.org/10.1093/cid/ciab411.
17. Liu Y, Liu J, Xia H, Zhang X, Fontes-Garfias CR, Swanson KA, Cai H, Sarkar R, Chen W, Cutler M, Cooper D, Weaver SC, Muik A, Sahin U, Jansen KU, Xie X, Dormitzer PR, Shi P-Y. 2021. Neutralizing activity of BNT162b2-

elicited serum. N Engl J Med 384:1466–1468. https://doi.org/10.1056/NEJMc2102017.
18. Georgiev IS, Joyce MG, Chen RE, Leung K, McKee K, Druz A, Van Galen JG, Kanekiyo M, Tsybovsky Y, Yang ES, Yang Y, Acharya P, Pancera M, Thomas PV, Wanninger T, Yassine HM, Baxa U, Doria-Rose NA, Cheng C, Graham BS, Mascola JR, Kwong PD. 2018. Two-component ferritin nanoparticles for multimerization of diverse trimeric antigens. ACS Infect Dis 4:788–796. https://doi.org/10.1021/acsinfecdis.7b00192.
19. Singh A. 2021. Eliciting B cell immunity against infectious diseases using nanovaccines. Nat Nanotechnol 16:16–24. https://doi.org/10.1038/s41565-020-00790-3.
20. Wang N, Shang J, Jiang S, Du L. 2020. Subunit vaccines against emerging pathogenic human coronaviruses. Front Microbiol 11:298. https://doi.org/10.3389/fmicb.2020.00298.
21. Jiang S, Bottazzi ME, Du L, Lustigman S, Tseng CTK, Curti E, Jones K, Zhan B, Hotez PJ. 2012. Roadmap to developing a recombinant coronavirus S protein receptor-binding domain vaccine for severe acute respiratory syndrome. Expert Rev Vaccines 11:1405–1413. https://doi.org/10.1586/erv.12.126.
22. He Y, Zhou Y, Liu S, Kou Z, Li W, Farzan M, Jiang S. 2004. Receptor-binding domain of SARS-CoV spike protein induces highly potent neutralizing antibodies: implication for developing subunit vaccine. Biochem Biophys Res Commun 324:773–781. https://doi.org/10.1016/j.bbrc.2004.09.106.
23. Du L, Zhao G, He Y, Guo Y, Zheng BJ, Jiang S, Zhou Y. 2007. Receptor-binding domain of SARS-CoV spike protein induces long-term protective immunity in an animal model. Vaccine 25:2832–2838. https://doi.org/10.1016/j.vaccine.2006.10.031.
24. Wang P, Nair MS, Liu L, Iketani S, Luo Y, Guo Y, Wang M, Yu J, Zhang B, Kwong PD, Graham BS, Mascola JR, Chang JY, Yin MT, Sobieszczyk M, Kyratsous CA, Shapiro L, Sheng Z, Huang Y, Ho DD. 2021. Antibody resistance of SARS-CoV-2 variants B.1.351 and B.1.1.7. Nature 593:130–135. https://doi.org/10.1038/s41586-021-03398-2.
25. Wu K, Werner AP, Moliva JI, Koch M, Choi A. 2021. mRNA-1273 vaccine induces neutralizing antibodies against spike mutants from global SARS-CoV-2 variants. bioRxiv 427948. https://doi.org/10.1101/2021.01.25.427948.
26. Muik A, Wallisch A-K, Sänger B, Swanson KA, Mühl J, Chen W, Cai H, Maurus D, Sarkar R, Türeci Ö, Dormitzer PR, Şahin U. 2021. Neutralization of SARS-CoV-2 lineage B.1.1.7 pseudovirus by BNT162b2 vaccine-elicited human sera. Science 371:1152–1153. https://doi.org/10.1126/science.abg6105.
27. Hussain M, Galvin HD, Haw TY, Nutsford AN, Husain M. 2017. Drug resistance in influenza a virus: the epidemiology and management. Infect Drug Resist 10:121–134. https://doi.org/10.2147/IDR.S105473.
28. Tan HX, Jegaskanda S, Juno JA, Esterbauer R, Wong J, Kelly HG, Liu Y, Tilmanis D, Hurt AC, Yewdell JW, Kent SJ, Wheatley AK. 2019. Subdominance and poor intrinsic immunogenicity limit humoral immunity targeting influenza HA stem. J Clin Invest 129:850–862. https://doi.org/10.1172/JCI123366.
29. Liu L, Nachbagauer R, Zhu L, Huang Y, Xie X, Jin S, Zhang A, Wan Y, Hirsh A, Tian D, Shi X, Dong Z, Yuan S, Hu Y, Krammer F, Zhang X, Xu J. 2017. Induction of broadly cross-reactive stalk-specific antibody responses to influenza group 1 and group 2 hemagglutinins by natural H7N9 virus infection in humans. J Infect Dis 215:518–528. https://doi.org/10.1093/infdis/jiw608.
30. Wang Z, Zhu L, Nguyen THO, Wan Y, Sant S, Quiñones-Parra SM, Crawford JC, Eltahla AA, Rizzetto S, Bull RA, Qiu C, Koutsakos M, Clemens EB, Loh L, Chen T, Liu L, Cao P, Ren Y, Kedzierski L, Kotsimbos T, McCaw JM, La Gruta NL, Turner SJ, Cheng AC, Luciani F, Zhang X, Doherty PC, Thomas PG, Xu J, Kedzierska K. 2018. Clonally diverse CD38+HLA-DR+CD8+ T cells persist during fatal H7N9 disease. Nat Commun 9 https://doi.org/10.1038/s41467-018-03243-7.
31. Rodda LB, Netland J, Shehata L, Pruner KB, Morawski PA, Thouvenel CD, Takehara KK, Eggenberger J, Hemann EA, Waterman HR, Fahning ML, Chen Y, Hale M, Rathe J, Stokes C, Wrenn S, Fiala B, Carter L, Hamerman JA, King NP, Gale M, Campbell DJ, Rawlings DJ, Pepper M. 2021. Functional SARS-CoV-2-specific immune memory persists after mild COVID-19. Cell 184:169–183.e17. https://doi.org/10.1016/j.cell.2020.11.029.
32. Dan JM, Mateus J, Kato Y, Hastie KM, Yu ED, Faliti CE, Grifoni A, Ramirez SI, Haupt S, Frazier A, Nakao C, Rayaprolu V, Rawlings SA, Peters B, Krammer F, Simon V, Saphire EO, Smith DM, Weiskopf D, Sette A, Crotty S. 2021. Immunological memory to SARS-CoV-2 assessed for up to 8 months after infection. Science 371 https://doi.org/10.1126/science.abf4063.
33. Zuo J, Dowell AC, Pearce H, Verma K, Long HM, Begum J, Aiano F, Amin-Chowdhury Z, Hallis B, Stapley L, Borrow R, Linley E, Ahmad S, Parker B, Horsley A, Amirthalingam G, Brown K, Ramsay ME, Ladhani S, Moss P. 2021. Robust SARS-CoV-2-specific T cell immunity is maintained at 6 months following primary infection. Nat Immunol 22.620–626. https://doi.org/10.1038/s41590-021-00902-8.
34. Gaebler C, Wang Z, Lorenzi JCC, Muecksch F, Finkin S, Tokuyama M, Cho A, Jankovic M, Schaefer-Babajew D, Oliveira TY, Cipolla M, Viant C, Barnes CO, Bram Y, Breton G, Hägglöf T, Mendoza P, Hurley A, Turroja M, Gordon K, Millard KG, Ramos V, Schmidt F, Weisblum Y, Jha D, Tankelevich M, Martinez-Delgado G, Yee J, Patel R, Dizon J, Unson-O'Brien C, Shimeliovich I, Robbiani DF, Zhao Z, Gazumyan A, Schwartz RE, Hatziioannou T, Bjorkman PJ, Mehandru S, Bieniasz PD, Caskey M, Nussenzweig MC. 2021. Evolution of antibody immunity to SARS-CoV-2. Nature 591:639–644. https://doi.org/10.1038/s41586-021-03207-w.
35. Li Q, Wu J, Nie J, Zhang L, Hao H, Liu S, Zhao C, Zhang Q, Liu H, Nie L, Qin H, Wang M, Lu Q, Li X, Sun Q, Liu J, Zhang L, Li X, Huang W, Wang Y. 2020. The impact of mutations in SARS-CoV-2 spike on viral infectivity and antigenicity. Cell 182:1284–1294.e9. https://doi.org/10.1016/j.cell.2020.07.012.
36. Inchauspe G, Vitvitski L, Major ME, Jung G, Spengler U, Maisonnas M, Trepo C. 1997. Plasmid DNA expressing a secreted or a nonsecreted form of hepatitis C virus nucleocapsid: comparative studies of antibody and T-helper responses following genetic immunization. DNA Cell Biol 16:185–195. https://doi.org/10.1089/dna.1997.16.185.
37. Wan J, Xing S, Ding L, Wang Y, Gu C, Wu Y, Rong B, Li C, Wang S, Chen K, He C, Zhu D, Yuan S, Qiu C, Zhao C, Nie L, Gao Z, Jiao J, Zhang X, Wang X, Ying T, Wang H, Xie Y, Lu Y, Xu J, Lan F. 2020. Human-IgG-neutralizing monoclonal antibodies block the SARS-CoV-2 infection. Cell Rep 32:107918. https://doi.org/10.1016/j.celrep.2020.107918.
38. Qiu C, Huang Y, Zhang A, Tian D, Wan Y, Zhang X, Zhang W, Zhang Z, Yuan Z, Hu Y, Zhang X, Xu J. 2013. Safe pseudovirus-based assay for neutralization antibodies against influenza virus A(H7N9) virus. Emerg Infect Dis 19:1685–1687. https://doi.org/10.3201/eid1910.130728.